

Paleoceanography and Paleoclimatology*



RESEARCH ARTICLE

10.1029/2024PA004936

Key Points:

- Multivariate Empirical Mode Decomposition is used to discern SST amplitude modulations at Milankovitch timescales in 17 ocean regions
- Causal inference highlights coupling between extratropical regions and both the Indian-Pacific Warm Pool and the Eastern Tropical Pacific
- Mechanisms are suggested linking global heat balance to ocean currents at multi-millennial timescales

Supporting Information:

Supporting Information may be found in the online version of this article.

Correspondence to:

T. Alberti,
tommaso.alberti@ingv.it

Citation:

Alberti, T., Stumpo, M., Florindo, F., & Rohling, E. J. (2025). Cause-and-effect relationships between sea surface temperature changes in different regions during the past 4.5 million years. *Paleoceanography and Paleoclimatology*, 40, e2024PA004936. <https://doi.org/10.1029/2024PA004936>

Received 31 MAY 2024

Accepted 10 JUN 2025

Cause-and-Effect Relationships Between Sea Surface Temperature Changes in Different Regions During the Past 4.5 Million Years

T. Alberti¹ , M. Stumpo², F. Florindo¹ , and E. J. Rohling^{3,4} 

¹Istituto Nazionale di Geofisica e Vulcanologia, Rome, Italy, ²Istituto di Astrofisica e Planetologia Spaziali, Rome, Italy, ³Faculty of Earth Sciences, Utrecht University, Utrecht, The Netherlands, ⁴School of Ocean and Earth Science, University of Southampton, Southampton, UK

Abstract Understanding long-term cause-and-effect relationships between changes at different locations and temporal scales is crucial for unraveling the key mechanisms that drive climate dynamics and their impacts on ecosystems and society. Here, we focus on deconvolving different modes of Sea Surface Temperature (SST) variability and the coupling between different ocean regions at timescales of orbital (Milankovitch) variability. To do so, we apply Multivariate Empirical Mode Decomposition (MEMD) and Linear Response Theory (LRT). Through MEMD, we identify significant SST amplitude modulations at Milankovitch timescales, correlations between oceanic regions, and a both spatially and temporally variable long-term cooling trend through the last 4 million years. Through LRT we assess nonlinear causal inference at different timescales, highlighting significant SST coupling between extratropical regions and both the Indian-Pacific Warm Pool and the Eastern Tropical Pacific at multi-millennial scales. Our methodology offers first insight into causal connections at different timescales and locations, and into how the large-scale redistribution of oceanic heat across latitudes, especially between equatorial and polar regions, potentially influences ocean circulation and, consequently, the observed pattern of SST fluctuations.

Plain Language Summary This study explores how changes in sea surface temperatures (SST) over millions of years affect different parts of the ocean and climate. By looking at data from various locations and time periods, we aim to advance understanding of the connections between ocean regions and the underlying mechanisms. Advanced techniques are used to analyze the data and it is found that SST changes are linked to natural cycles of orbitally induced insolation change, known as Milankovitch cycles, which occur over tens of thousands of years. We also reveal a variable long-term cooling trend over the past 4 million years, and interactions between sea surface temperatures in different ocean regions over thousands of years. Based on our new results, we suggest possible mechanisms through which the large-scale redistribution of oceanic heat across latitudes, especially between equatorial and polar regions, potentially influences ocean currents, shaping long-term SST patterns.

1. Introduction

Over the past 4.5 million years (Myr), the Earth has undergone significant long-term cooling, as a part of a trend that began ~15 million years ago (Ma) at the termination of the Mid-Miocene Climatic Optimum (Foster et al., 2012; Herbert et al., 2022; Herold et al., 2012; Holbourn et al., 2013; Meckler et al., 2022; Ravelo et al., 2004; Rohling et al., 2022). During the past 4.5 Myr, several major climate transitions occurred within the context of that long-term cooling, including the intensification of Northern Hemisphere (NH) glaciation around 2.5–3 Ma and a shift from ~41 to ~100 kyr variability during the Middle Pleistocene Transition (MPT) from ~1,250 to 750 ka (Berends et al., 2021; Herbert, 2023; Westerhold et al., 2020).

Understanding the evolution of Plio-Pleistocene climate in response to orbital forcing remains a significant challenge in climate science, partly because of uncertainties in temperature and sea level reconstructions that hinder a comprehensive explanation of the mechanisms driving ice sheet-climate interactions and their relationship with orbital forcing (Ashkenazy & Tziperman, 2004; Daruka & Ditlevsen, 2016; Ditlevsen & Ashwin, 2018; Hays et al., 1976; Imbrie et al., 1993; Lisiecki & Raymo, 2005; Paillard & Parrenin, 2004).

© 2025. The Author(s).

This is an open access article under the terms of the [Creative Commons Attribution License](https://creativecommons.org/licenses/by/4.0/), which permits use, distribution and reproduction in any medium, provided the original work is properly cited.

Table 1
The List of All SST Regions Along With Their Corresponding Boundaries and Locations

SST region	Latitude	Longitude
Northern Hemisphere	0°–90°N	0°–360°
Southern Hemisphere	0°–90°S	0°–360°
NH Extratropics	23.5°N–90°N	0°–360°
SH Extratropics	23.5°S–90°S	0°–360°
Tropics	23.5°S–23.5°N	0°–360°
Indo-Pacific Warm Pool (IPWP)	15°S–15°N	90°E–180°E
Eastern Tropical Pacific (ETP)	10°S–5°N	150°W–90°W
Subtrop upwelling	10°N–30°N	100°W–80°W
Eq upwelling	5°S–5°N	140°W–90°W
Warm pool	10°S–10°N	120°E–170°E
North Atlantic (Natl)	0°–60°N	80°W–0°
Tropical Atlantic (tropAtl)	5°S–5°N	40°W–20°W
South Atlantic (Satl)	0°–30°S	50°W–10°E
North Pacific (Npac)	0°–60°N	120°E–100°W
South Pacific (Spac)	0°–30°S	150°E–80°W
Tropical Pacific (tropPac)	5°S–5°N	160°E–90°W

Much of the understanding of global climate change through the Cenozoic relies on $\delta^{18}\text{O}$ records of benthic foraminifera (e.g., Cramer et al., 2011; Emiliani, 1955; Lisiecki & Raymo, 2005; Miller et al., 1991; Ravelo & Hillaire-Marcel, 2007; E. Rohling & Cooke, 1999; Westerhold et al., 2020; Zachos et al., 2001). This isotopic record encompasses a composite signal derived from local water temperature variations and the $\delta^{18}\text{O}$ composition of seawater ($\delta^{18}\text{O}_{\text{sw}}$) (Shackleton, 1987). Based on $\delta^{18}\text{O}$ records it has been demonstrated that the waxing and waning of ice sheets during the Pleistocene was governed by insolation distribution and intensity variations due to changes in Earth's orbital configuration at Milankovitch timescales (20–100 kyr). These orbital forcing mechanisms, interacting with the carbon cycle, land cover, ocean circulation, and other Earth system components, translated into deep-sea temperature shifts of 4–6°C and sea level fluctuations of up to 135 m (Berends et al., 2021; Rohling et al., 2022). However, systematic assessments of sea surface temperature (SST) records from diverse ocean regions and associated SST gradients are lacking, which impedes a comprehensive understanding of orbital-scale changes in oceanic temperatures (Clark et al., 2024; Rohling et al., 2014, 2021).

Recently, Clark et al. (2024) aimed to address these issues, and compiled sea surface temperature (SST) records based on 128 published records of alkenone, Mg/Ca, and faunal proxy time series to reconstruct global and regional temperature differences throughout the past 4.5 Myr relative to the late Holocene. This compilation provides a framework for understanding global temperature evolution independent of $\delta^{18}\text{O}$ records.

Here, we extend the scope of previous investigations by combining the data-adaptive Multivariate Empirical Mode Decomposition (MEMD) method (Rehman & Mandic, 2010) to explore SST variability between different ocean regions at Milankovitch timescales, with Linear Response Theory (Baldovin et al., 2020) to unravel intricate cause-and-effect relationships between changes at different locations and temporal scales.

2. Data and Methods

2.1. Data

We use the SST record compilation of Clark et al. (2024) at 1 kyr temporal resolution. They analyzed long-term temperature evolution over the last 4.5 Myr and stacking them within latitude bands. This produced comprehensive SSTs records (with their 1- σ uncertainty) for 17 different locations (see Clark et al. (2024)) placed on the LR04 age model (Lisiecki & Raymo, 2005) whose orbital tuning has been alleviated by using an independent depth-derived age model over the corresponding $\delta^{18}\text{O}$ record for each location (Clark et al., 2024). In the following we analyze all 17 records (see Table 1 for the full list and location), but specifically focus on those from four selected regions (Figure 1), that is, Northern Hemisphere (NH) extratropics, IPWP (Indo-Pacific Warm Pool), ETP (eastern tropical Pacific), and Equatorial upwelling, to illustrate the main findings of our analysis. These regions were selected due to their roles in the global climate system. The NH extratropics provide insights into atmospheric and oceanic circulation patterns, while the IPWP is crucial for understanding tropical ocean-atmosphere interactions, including tele-connection phenomena and patterns (as El Niño and La Niña phenomena). The ETP is vital for studying ENSO dynamics, and equatorial upwelling is important for ocean productivity and carbon cycles.

2.2. Multivariate Empirical Mode Decomposition

MEMD (Rehman & Mandic, 2010), an extension of univariate EMD (Huang et al., 1998), belongs to the category of adaptive decomposition methods (Huang & Wu, 2008). Like EMD, MEMD enables deconvolution of a set of observables $s(t)$ (e.g., the 17 SST records) into a finite number n_k of oscillating patterns $c_k(t)$, referred to as Multivariate Intrinsic Mode Functions (MIMFs), along with a monotonic residue $r(t)$, as expressed by:

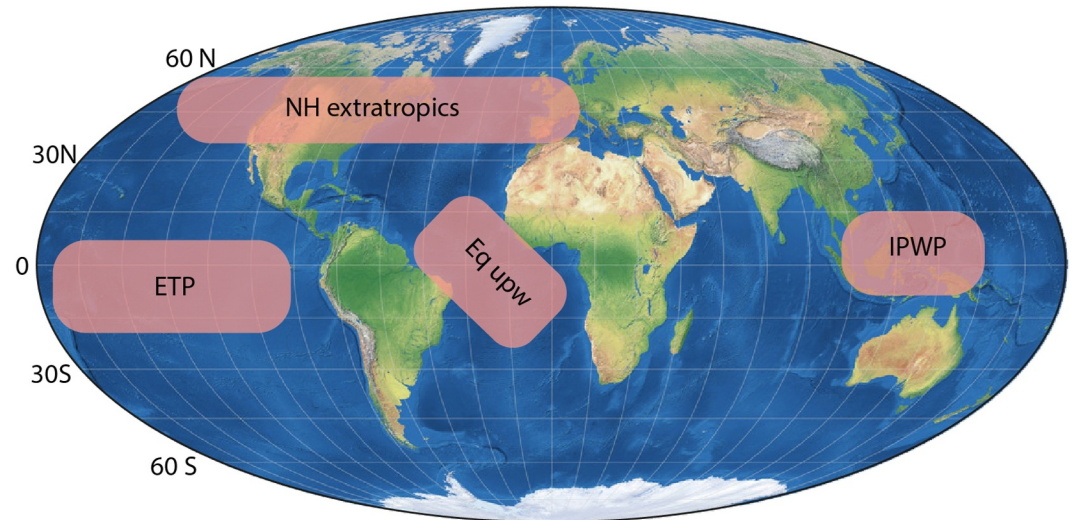


Figure 1. Locations of the four selected regions used in this study.

$$s(t) = \sum_{k=1}^{n_k} c_k(t) + r(t). \quad (1)$$

The MIMFs are obtained through a sifting process (Huang et al., 1998), where local extremes of $s(t)$ are first identified, then interpolated via cubic splines to derive upper and lower envelopes $u(t)$ and $\ell(t)$, respectively (Rehman & Mandic, 2010). A mean envelope $m(t) = (u(t) + \ell(t))/2$ is derived, and the detail $h(t) = s(t) - m(t)$ is evaluated. The first MIMF is obtained if the detail $h(t)$ has the same (or differing by one) number of local extremes and zeros, along with a zero-average mean envelope. Iteration of the sifting process continues until these criteria are met (Lovati et al., 2023; Rehman & Mandic, 2010). The process halts when no further MIMFs can be extracted, yielding the monotonic non-oscillating residue $r(t)$ (Alberti, Consolini, et al., 2020; Alberti, Giannattasio, et al., 2020; Alberti et al., 2021; Rehman & Mandic, 2010).

MEMD offers a system representation as a sum of fluctuating contributions at different average timescales (Huang & Wu, 2008), where each contribution is a non-stationary function with time-dependent amplitude and phase, expressed as $c_k(t) = a_k(t) \cos[\phi_k(t)]$. The instantaneous amplitude $a_k(t)$ and phase $\phi_k(t)$ are derived using the Hilbert transform (Huang et al., 1998; Huang & Wu, 2008), while instantaneous and average timescales are determined as $T_k(t) = \frac{1}{2\pi} \left(\frac{d\phi_k(t)}{dt} \right)^{-1}$ and $\langle T \rangle = \langle T_k(t) \rangle$. Further details can be found in Huang et al. (1998), Huang and Wu (2008), Rehman and Mandic (2010), Alberti et al. (2014).

For the 17 SST records, MEMD derived a set of 7 MIMFs whose average timescales $\langle T \rangle$ with errors as standard deviations are reported in Table 2. It is interesting to note that all Milankovitch timescales related to precession (~ 21 kyr), obliquity (~ 41 kyr), and eccentricity (~ 100 kyr) can be recognized through MIMFs 5, 6, and 7, respectively. Small-scale cycles (up to the order of 10 kyr) are also noted.

2.3. Causality and Linear Response Theory

Exploring how changes in one or more system variables cause changes in other variables is a central topic in complex systems analysis (Baldovin et al., 2020; Schreiber, 2000; Stumpo et al., 2020, 2023). While correlation implies a statistical relationship between two or more variables, it does not (necessarily) imply causation. Two variables can be correlated due to the

Table 2
Average Timescales $\langle T \rangle$ With Errors as Standard Deviations for Each MIMF

MIMF number	Average timescales $\langle T \rangle$ (kyr)
1	2.8 ± 0.1
2	4.9 ± 0.1
3	8.7 ± 0.2
4	13.0 ± 0.3
5	23.4 ± 0.9
6	41 ± 2
7	96 ± 5

common effects of a third variable, even if they are not causally related. This can be simply described via the system Equations 2–4.

$$x_{t+1} = \alpha x_t + \beta \eta_t \quad (2)$$

$$y_{t+1} = \alpha x_t + \alpha y_t + \beta \eta_t \quad (3)$$

$$z_{t+1} = \alpha x_t + \alpha z_t + \beta \eta_t \quad (4)$$

In which y_t and z_t , although correlated, are not causally linked (they are simply subject to the same common driver, x_t). By considering a more general N-dimensional linear system

$$\mathbf{x}_{t+1} = \mathbf{F}(\mathbf{x}_t) \quad (5)$$

where $\mathbf{x}_t = \{x^{(1)}, x^{(2)}, \dots, x^{(N)}\}$ is a N-dimensional state variable and \mathbf{F} describes the temporal evolution of the system. Causation, in its interventional sense that accounts for effects of external actions on the system between two variables $x^{(j)}$ and $x^{(k)}$, occurs when a perturbation on $x^{(j)}$ at $t = 0$ leads, on average, to a change on $x^{(k)}$ at $t = \tau > 0$. By combining this concept with linear response theory (LRT) Baldovin et al. (2020) introduced a metric of causation R_τ^{kj} , that is, the response matrix,

$$R_\tau^{kj} \doteq \lim_{\delta x_0^{(j)} \rightarrow 0} \frac{\delta \bar{x}_\tau^{(k)}}{\delta x_0^{(j)}} = - \left\langle x_\tau^{(k)} \frac{\partial \ln p_s(\mathbf{x})}{\partial x^{(j)}} \Big|_{\mathbf{x}_0} \right\rangle \quad (6)$$

provided that $p_s(\mathbf{x})$ is the stationary invariant probability distribution function (pdf) of the system $\{\mathbf{x}_t\}$ that is known a priori or can be inferred from data. The average in Equation 6 is performed over the two-times joint pdf $p_s^{(2)}(\mathbf{x}, \mathbf{x}_0)$. In case of linear systems there are no constraints on the amplitude of $\delta x_0^{(j)}$, while for nonlinear systems it must be that $|\delta x_0^{(j)}| \ll |x_0^{(j)}|$. Equation 6 provides a simple way to determine direct and indirect causation relations between $x^{(j)}$ and $x^{(k)}$ at different times τ . In particular, for Markov linear systems (such as the system Equations 2–4), the response matrix in Equation 6 can be evaluated as

$$R_\tau = C_\tau C_{\tau_0}^{-1}, \quad (7)$$

where $C_\tau = \langle \mathbf{x}_\tau \mathbf{x}_0 \rangle$ is the covariance matrix, and $C_{\tau_0}^{-1}$ is its inverse at initial time $\tau = \tau_0$ (Baldovin et al., 2020). We remark that $R_{\tau_0}^{kj} \neq 0$ only if *direct* (*direct/indirect* for $\tau > \tau_0$) causation exists from \mathbf{x}^j to \mathbf{x}^k , in contrast to cross correlation analysis. In this study, the causation metric relies on Equation 7. In our case, $x^{(j)}$ and $x^{(k)}$ represent a given timescale component of SST records at different locations, respectively, allowing us to explore mutual causal coupling between temperature changes in different ocean regions at different times τ . The latter is representative of the temporal delay of the response in the region k , monitored via $x^{(k)}$, following a change τ kyr earlier in region j , monitored via $x^{(j)}$.

We remark that Equation 7 is based on the assumption that the system is Markov linear, which is a necessary condition for any causal inference analysis. Indeed, in terms of stochastic processes the Markov condition is equivalent to requiring the knowledge of the whole set of variables describing a system (i.e., there are no hidden variables), such that the causal links among variables are not spurious. For this purposes, Markovianity is usually referred to the multi-component system and not to the single variables taken alone. For example, if we consider a Brownian particle immersed in an inhomogeneous external field, then the velocity of the particle would depend on the external force and implicitly also on the particle position. Given that the particle position depends on the velocity at all previous times, the velocity itself depends implicitly on its values at all previous times. Thus, the velocity alone is a non-Markov process. Nevertheless, the two-component process is Markovian (Van Kampen, 1992). Then, although we cannot be confident that each SST record is Markovian, we can easily assume that the whole set of SST records is descriptive enough of the system (i.e., they form a Markov system since they provide knowledge on the dynamical variables). This is the best we can do in practice in absence of a dynamical model.

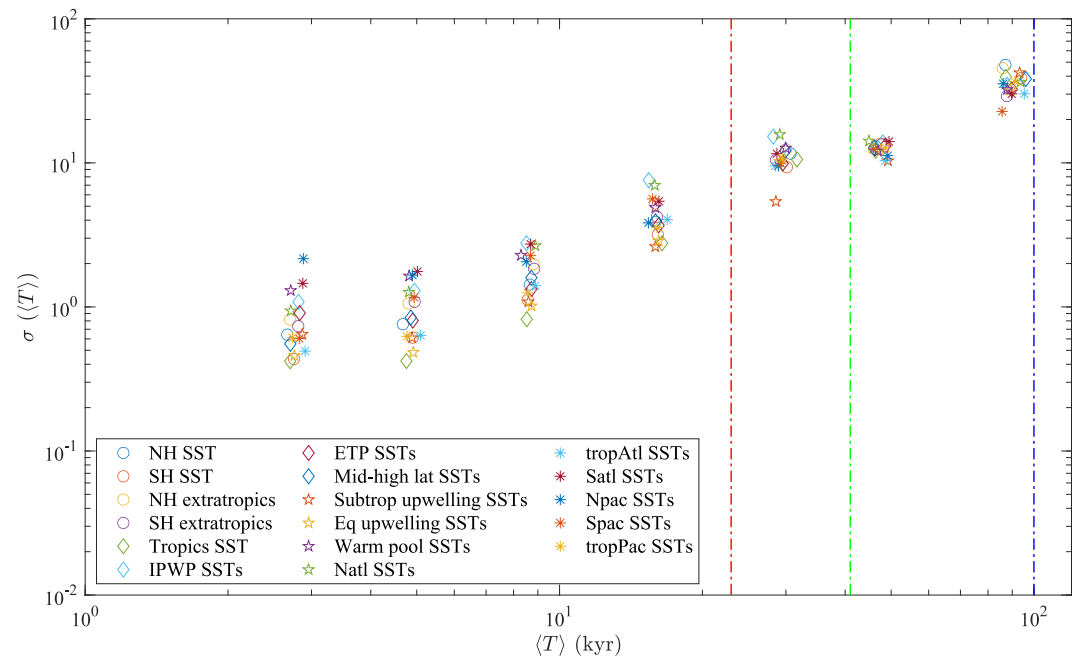


Figure 2. The percentage variance of each empirical mode for the different records as a function of the average timescale. Dashed lines refer to the Milankovitch orbital cycles of precession (red), obliquity (green), and eccentricity (blue).

Furthermore, regarding the assumption of linear dynamics, Baldovin et al. (2020) thoroughly investigated Equation 7 for the inference of causality also in nonlinear systems and concluded that, although the causal strength is overestimated, the error is bounded. Thus, meaningful causal relations can be obtained if the nonlinear contribution is small enough (Baldovin et al., 2020). However, to further address this issue we tested the causality obtained through Equation 7 for paired SSTs interaction (i.e., NH extratropics \rightarrow Eq upwelling at the Milankovitch timescale of 41 kyr) with the results obtained from a nonlinear causal method, that is, the transfer entropy (TE) (Schreiber, 2000). We found consistent results in terms of both causal links and estimation of time delays (not shown) between the two methods. However, the LRT-based method is straightforward for the multivariate analysis. Other methods, such as the TE, are not as straightforward because the inference of N -dimensional probability distributions is required, where N is the number of variables considered ($N = 17$ in our case). For this reason, a huge amount of data would be necessary, which unfortunately are not available in the context of SST records (and paleoclimate records in general). However, the possibility of including the whole set of the 17 SST records is crucial to make the system as complete as possible in terms of Markov condition. This makes the LRT-based method preferable over the TE (or other methods) in our case.

Finally, we remark that causal consistency is tacitly assumed in this work, which means that the causal strength estimated through Equation 7 is averaged over the whole time range of the data set. In principle, it would be possible to perform a time-windowed analysis. However, that would require a larger data set in order to have sufficient statistics in any time window. For this reason we decided to limit our analysis to the inference of averaged causal links over the full time range. Furthermore, use of the MEMD allows us to fully account for the $1-\sigma$ uncertainty on data (Clark et al., 2024). MEMD, acting as a dyadic filter (Huang & Wu, 2008), filters out noise content and uncertainty in the first MIMF, highlighting how MEMD can effectively assist in removing uncertainties and smoothing other modes before performing causal inference analysis. Furthermore, since our analysis focuses on Milankovitch timescales, which are significantly longer than the timescale of the first MIMF, our results regarding causality remain robust, even in the presence of uncertainties in the raw data.

3. Results

It has been suggested that NH glacial intensification and the MPT occurred almost independently of orbital forcings, via a frequency-locking mechanism (Ashwin & Ditlevsen, 2015; Daruka & Ditlevsen, 2016), although Pleistocene climate variability is mainly dominated by the 41 kyr obliquity cycle before the MPT and by ~ 100 kyr

dynamics after the MPT (Ashkenazy & Tziperman, 2004; Hays et al., 1976; Imbrie et al., 1993). Our inspection of energy-timescale variability in the oceanic regions during the past 4.5 Myr (Figure 2) indicates dominant variance (~40%) at the eccentricity timescale, decreasing to about 15% for both precession and obliquity cycles, and shorter timescales.

The residual of the deconvolution ($r(t)$ in Equation 1), which can be interpreted as long-term trend variability, indicates global cooling over the last 4 million years (Myr) (Figure 3), although with different rates of acceleration (i.e., slower for the Indo-Pacific Warm Pool region). Although our results are quantitatively in agreement with the linear trend extracted by Clark et al. (2024) in terms of their cooling, the adaptive nature of the MEMD allows us to extract nonlinear monotonic residuals, and thus to better represent their temporal variations. These residuals reveal (Figure 3) increased cooling rates before and during the MPT, and decreased cooling rates after the MPT (the last 700 kyr). The NH extratropics, eastern tropical Pacific (ETP), and equatorial upwelling regions are all characterized by similar cooling trends.

Besides the long-term trend variability, we are interested in evaluating temperature coupling between the oceanic regions at different temporal scales, with a specific focus on Milankovitch timescales. We observe a slight increase in SST amplitude modulation at precession timescales during the MPT, in the equatorial upwelling and ETP regions (Figures 4A1–4A3), with respect to the period between 2 and 4 Ma. Conversely, there is no evidence of amplitude modulation at the obliquity timescale (Figures 4B1–4B3), in contrast with the dominance of 41-kyr amplitude variability before the MPT and its decrease after the MPT in benthic $\delta^{18}\text{O}$ stacks (Ditlevsen & Ashwin, 2018; Huybers & Wunsch, 2004; Lisiecki & Raymo, 2005). At eccentricity timescales (Figures 4C1–4C3), we observe SST amplitude modulation over the last 4 Myr, with amplitude increasing prior to and after the MPT for different oceanic regions. Similar amplitude variability across the MPT has been noted in Antarctic ice core $\delta^{18}\text{O}$ (Daruka & Ditlevsen, 2016; Ditlevsen & Ashwin, 2018). Our results point toward possible coherence between variabilities in different regions at Milankovitch timescales.

To quantify to what extent evolving surface warming patterns at different timescales in a specific region can lead to temperature changes in other regions, we analyze causation using linear response theory. The main findings for causation at different scales for three selected regions (i.e., the NH extratropics and (a) IPWP, (b) ETP, and (c) Equatorial upwelling) are shown in Figure 5, while the causation at different timescales and for all regions is illustrated in Supplementary Movies. Note that, although only three selected regions (referred to as variables) are shown, the response matrix in Equation 7 was computed for the entire set of variables (with the remainder being referred to as hidden variables). This approach allows us to avoid any spurious causality due to “common drivers” that might be contained in the hidden variables.

Timescales <5 kyr (i.e., MIMFs 1–2; Movies S1 and S2) show no significant coupling between different regions. At timescales shorter than the precession cycle (i.e., IMFs 3–4, $\langle T \rangle$ –9–13 kyr), we instead detect a significant coupling between some specific regions as outlined below.

At the ~9 kyr timescale (see Movie S3), Southern Hemisphere (SH) SSTs appear to causally influence variability in tropical SSTs—particularly in the Eastern Tropical Pacific (ETP)—and equatorial upwelling SSTs, with a time lag of approximately 1,000–3,000 years (Figure 6a). While changes in the Atlantic Meridional Overturning Circulation (AMOC) associated with millennial-scale events such as Heinrich or Dansgaard-Oeschger cycles can induce rapid interhemispheric heat redistribution and synchronise temperature changes across distant regions, this mechanism alone may not fully account for the observed lag. The delay could instead reflect the combined influence of slower processes, including adjustments in deep ocean heat storage, oceanic wave propagation, and shifts in Southern Hemisphere westerly winds, which affect the upwelling dynamics in the equatorial Pacific. These additional mechanisms may introduce a multi-step transmission of climate signals from the Southern Ocean to the tropics, thus contributing to the multi-centennial to millennial-scale delay in tropical SST responses.

At the ~13 kyr timescale (see Movie S4), extratropical SST changes appear to causally lead SST variations in both NH and SH mid-to-high latitudes—especially in the North Atlantic—with a time delay of approximately 5–8 kyr (Figure 6b). SST variations in extratropical regions relate to heat redistribution from equatorial areas toward higher latitudes, influencing regional and global climate patterns. However, the long lag observed challenges a simple interpretation based solely on AMOC dynamics. While AMOC-related processes likely contribute, additional mechanisms—such as slow feedbacks involving sea ice extent, albedo, ocean stratification, and long-term heat storage—may also play a role over these timescales. The delay may reflect the cumulative and nonlinear

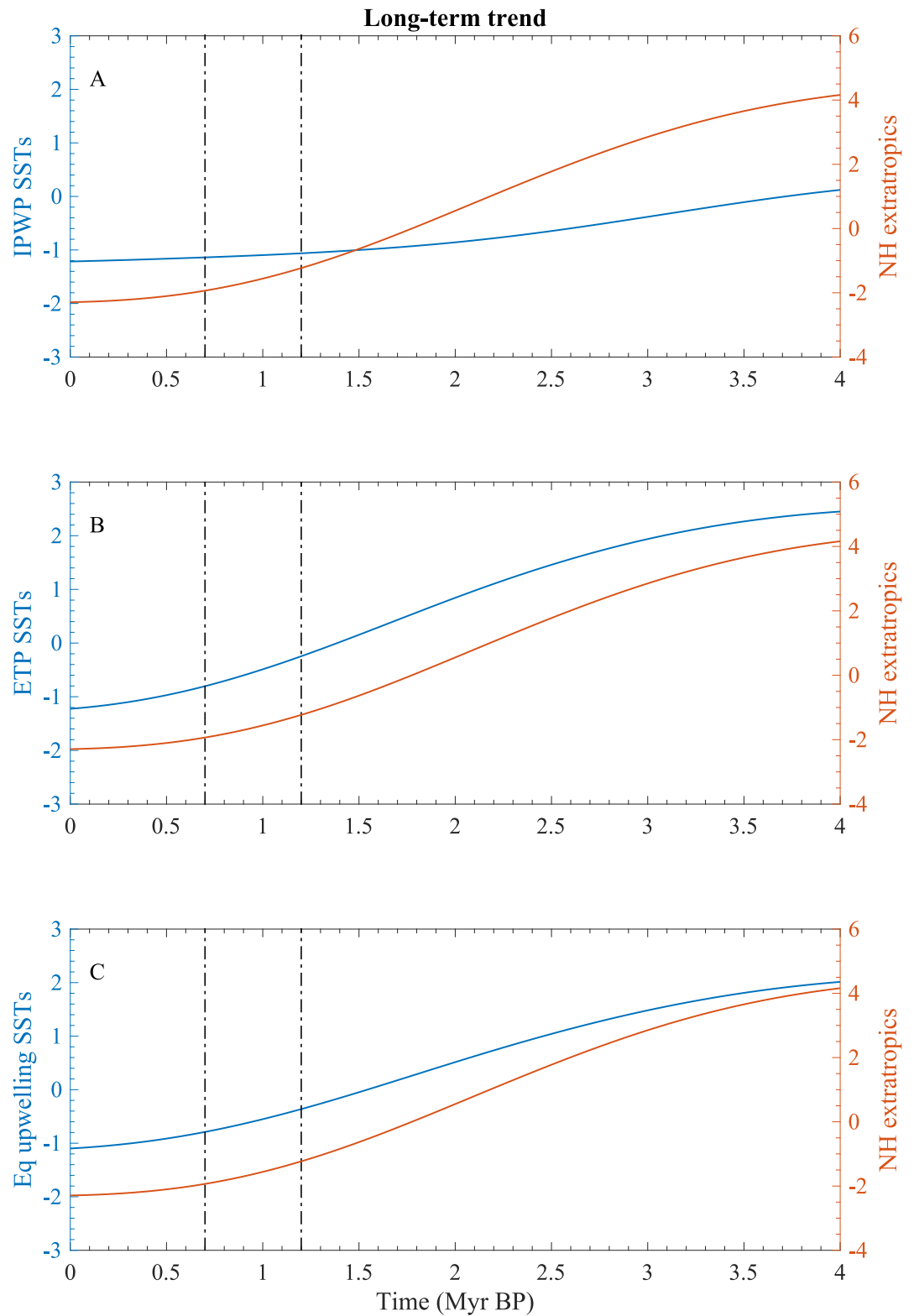


Figure 3. Long-term trends for the NH extratropics SST (red lines) in comparison with those extracted from (a) IPWP, (b) ETP, and (c) Equatorial upwelling. Vertical dashed lines identify the MPT as in Clark et al. (2006).

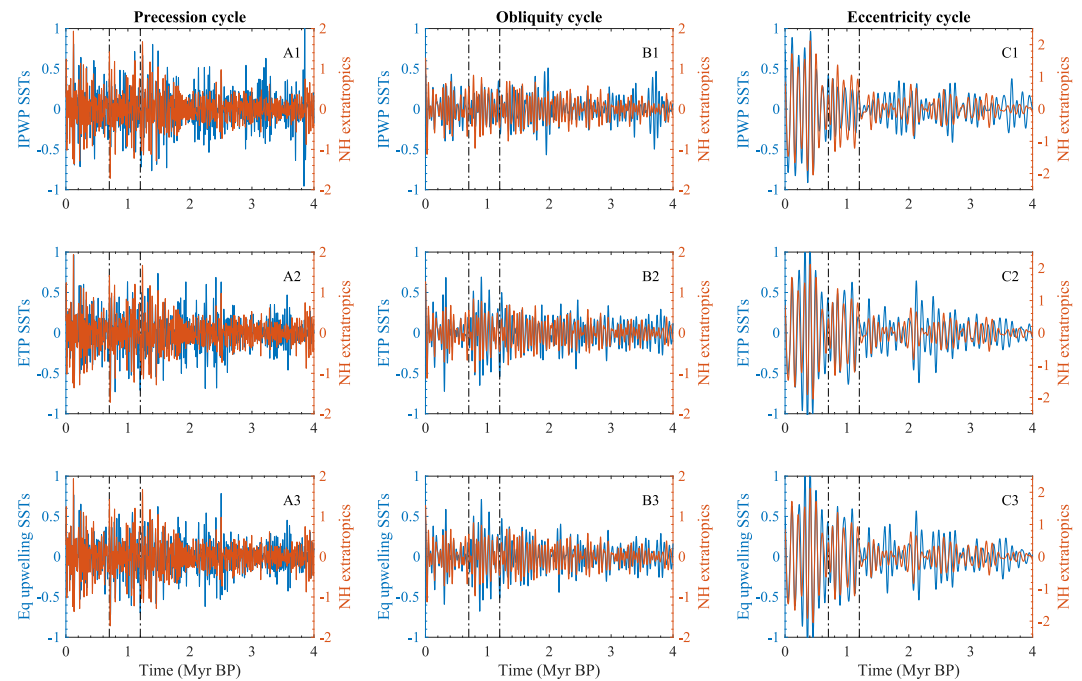


Figure 4. The Milankovitch cycles (precession, obliquity, and eccentricity) for the NH extratropics SST (red lines) in comparison with those extracted from (a) IPWP, (b) ETP, and (c) Equatorial upwelling. Vertical dashed lines identify the MPT as in Clark et al. (2006).

response of the thermohaline circulation (THC) to orbital forcing and internal climate variability, which requires further investigation through dynamic modeling.

At both precession (23 kyr) and obliquity (41 kyr) timescales (i.e., MIMFs 5–6; Movies S5 and S6), we observe that NH extratropical SST variations causally lead SST fluctuations in the IPWP, tropical, and subtropical regions, with time delays between 6 and 13 kyr (Figure 6c). These results likely reflect how changes in the distribution of solar radiation across latitudes affect the intensity and location of heating and cooling within the atmosphere and oceans (Brierley et al., 2009). We find that the latitudes most affected by these insolation-driven changes are typically the high and mid-latitudes, with subsequent impacts on ocean heat redistribution. As an example, during periods of high obliquity, latitudes closer to the poles receive more solar radiation during summer, leading to enhanced warming and increased melting of polar ice. Conversely, during periods of low obliquity, the polar regions experience less solar radiation and cooler temperatures. Also, the sign of obliquity-related insolation forcing flips over at $\sim 40^\circ$ of latitude, so that pole-to-equator contrasts are affected even more (see illustration in E. J. Rohling et al. (2012), their Figure 8). The long causality delays and leading role of high-latitude variations we find on these timescales are, therefore, likely related to the role of the large-scale redistribution of oceanic heat across latitudes in the strength and extent of oceanic circulation patterns, with a focus on the thermohaline circulation.

At eccentricity timescales (100 kyr, MIMF 7; Movie S7), we observe an opposite behavior (Figure 6d), with tropical changes leading and causing changes in almost all other regions, with time delays of about 10–13 kyr, reaching maximum values for causal strength at precession timescales (23 kyr). We propose that this reflects the role of eccentricity in modulating the amplitude of precession influences (seasonal and hemispheric contrasts).

While these interpretations are consistent with our results and current understanding of large-scale ocean–atmosphere interactions, we acknowledge that some of the lead-lag relationships—particularly those involving multi-kyr delays—remain only partially understood. These findings should therefore be viewed as hypotheses that flag key regions and timescales for future process-based and dynamical investigations. Table 3 summarizes the inferred lead-lag relationships at different timescales among the presented oceanic regions.

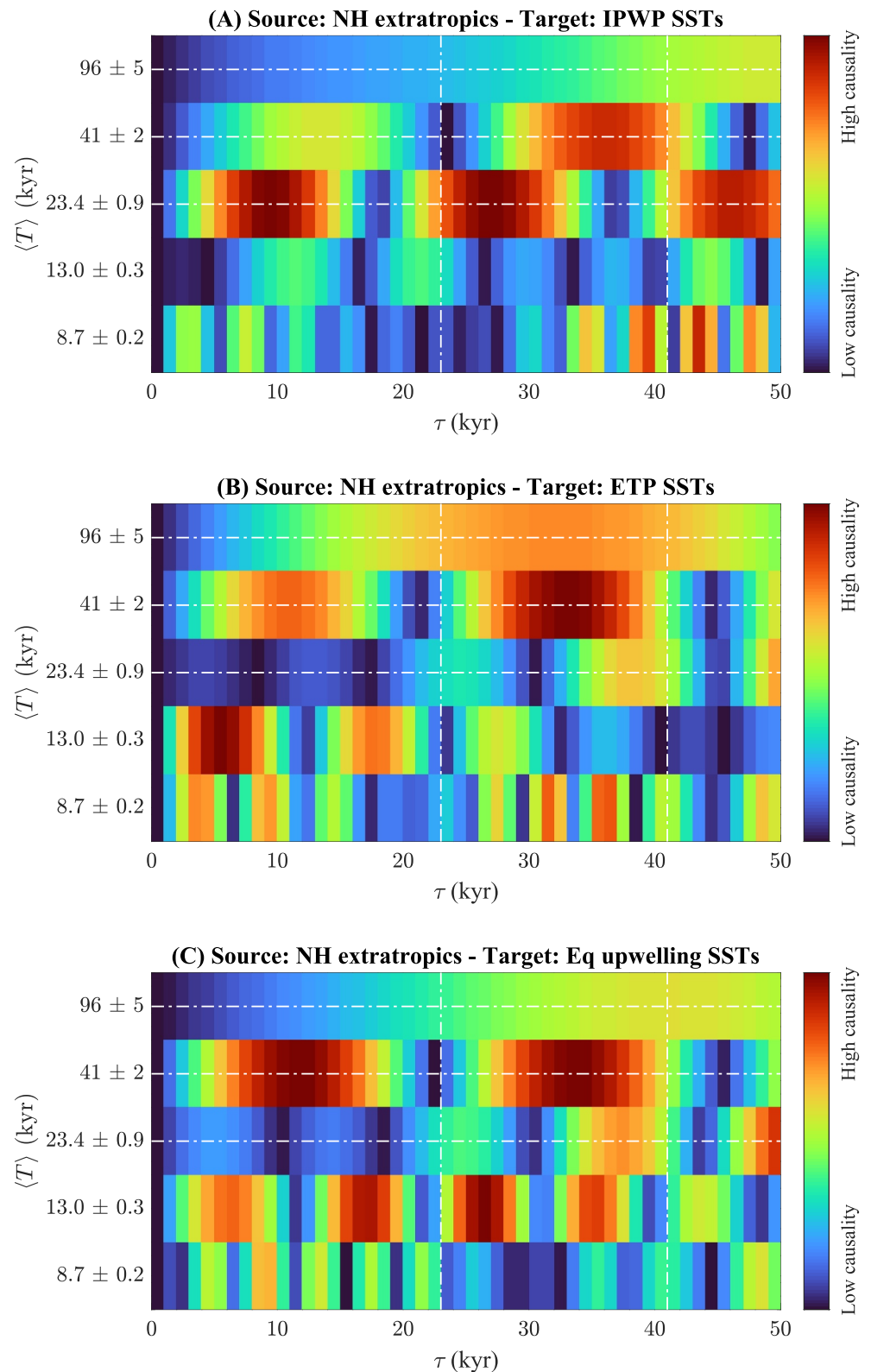


Figure 5. Causality strengths between the NH extratropics and (a) IPWP, (b) ETP, and (c) Equatorial upwelling at different timescales (y axis) and temporal delays (x axis). Dashed lines refer to the Milankovitch cycles (precession, obliquity, and eccentricity).

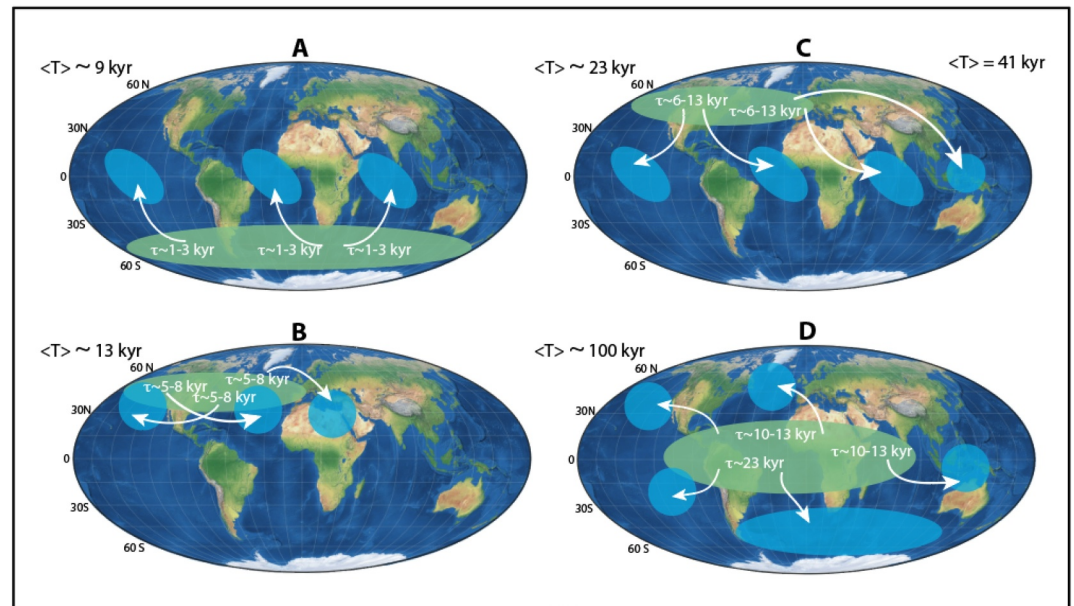


Figure 6. Conceptual illustration depicting the multi-scale causal relationships between oceanic regions and climate variables, as described in the text. Arrows denote the direction of causation, with varying time delays observed across different timescales, reflecting the interconnected dynamics of Earth's climate system. Green areas correspond to regions that lead causal variations to the others reported in blue. Areas correspond to those described in the text. (a) timescale $\tau \sim 9 \text{ kyr}$; (b) timescale $\tau \sim 13 \text{ kyr}$; (c) timescale $\tau \sim 23\text{--}41 \text{ kyr}$; (d) timescale $\tau \sim 100 \text{ kyr}$.

4. Conclusions and Outlook

We aim to disentangle the complex interplay between orbital forcing, ocean dynamics, and global climate evolution during the Plio-Pleistocene. We employ the compilation of SST records assembled by Clark et al. (2024) as a framework for understanding global temperature evolution. We analyze this compilation using MEMD and LRT, to explore SST variability between different oceanic regions at Milankovitch timescales and unravel cause-and-effect connections.

The causal inference framework adopted here is based on the hypothesis that the underlying system can be treated as a high-dimensional Markov process. We remark again that Markovianity is a necessary condition for any causal inference analysis, such as the Momentary Information Transfer (MIT), TE and so forth. Requiring the Markov condition is equivalent to suppose that the set of dynamical variables contains all the relevant information of the system (i.e., there are no hidden variables). While we acknowledge that no set of paleoclimate records can offer a complete description of Earth system dynamics, we argue that our use of 17 SST time series from geographically distinct regions provides a sufficiently rich approximation of the system's state vector to capture its dominant modes of variability. Although some unobserved confounders may exist, their effect is likely minimized when a large, well-distributed set of system variables is included. Another caveat of the LRT method is the assumption that the coupling is linear. We did not use nonlinear frameworks directly because they require the estimation of high-dimensional probability distributions and a huge amount of data would be necessary (that are not available). We verified the robustness of our results by comparing the LRT-based method with a nonlinear approach based on TE, both applied to 2×2 subsystems (e.g., NH extratropics \leftrightarrow Eq upwelling at the Milankovitch timescale of 41 kyr). The comparison yielded consistent causal directions and delays for selected region pairs, confirming the validity of our

Table 3
Summary of the Inferred Lead-Lag Relationships at Different Timescales Among the Presented Oceanic Regions

Average timescales $\langle T \rangle$ (kyr) – 9 kyr	
Causal relationship	Time delay τ (kyr)
SH \rightarrow ETP	1–3
SH \rightarrow Eq upwelling	1–3
Average timescales $\langle T \rangle$ (kyr) – 13 kyr	
Causal relationship	Time delay τ (kyr)
Extratropics \rightarrow NH	5–8
Extratropics \rightarrow SH	5–8
Average timescales $\langle T \rangle$ (kyr) – 23 and 41 kyr	
Causal relationship	Time delay τ (kyr)
NH extratropics \rightarrow IPWP	6–13
NH extratropics \rightarrow tropics	6–13
NH extratropics \rightarrow sub-tropics	6–13
Average timescales $\langle T \rangle$ (kyr) – 100 kyr	
Causal relationship	Time delay τ (kyr)
Tropics \rightarrow other regions	10–13

conclusions within current data constraints. The results of this comparison are consistent with the analysis reported by Baldovin et al. (2020), showing that, in the case of nonlinear systems, the LRT method slightly overestimates the causal strength, although the error is bounded. Nevertheless, we acknowledge that the potential influence of unobserved variables represents source of uncertainty. Therefore, the inferred relationships should be interpreted as statistically significant but still subject to further validation, ideally via models or higher-resolution data sets. Our findings are summarized below.

We identify a ubiquitous long-term cooling trend over the past 4 million years, except in the IPWP region, where temperatures remained relatively constant. We also identify causal relationships (Figure 6) between oceanic regions, with extratropical SST variations influencing equatorial upwelling and mid-to-high latitude SST changes at ~9–13 kyr timescales. Although our study does not aim to directly resolve the lead-lag dynamics or the full physical processes governing ocean heat balance and circulation changes, our statistical findings are consistent with several hypothesized mechanisms that may help interpret the observed patterns. These include: (a) Atlantic Meridional Overturning Circulation (AMOC) variability and its nonlinear responses to external forcing (Jackson et al., 2015), (b) tropical-extratropical coupling via wave dynamics and atmospheric tele-connections, (c) feedbacks involving sea ice and deep ocean circulation, and (d) potential nonlinear thresholds or tipping points in ocean circulation (Lenton et al., 2008). Clarifying these mechanisms is important to avoid misinterpretation of our statistical results and to provide a plausible physical context for them. Indeed, the observed patterns are coherent with multi-millennial-scale alterations in insolation distribution, impacting wind intensities and consequently influencing ocean surface circulation.

Changes in SST at mid-to-high latitudes are indicative of oceanic heat redistribution, which in turn influences deeper ocean layers through the THC over millennia, with the Atlantic Meridional Overturning Circulation (AMOC) potentially responding to climate forcing through multiple stable states, hysteresis, and nonlinearities. Our findings suggest that variations in the global heat balance between low and high latitudes may trigger shifts between these states, affecting oceanic heat distribution.

At precession and obliquity timescales, we find that NH extratropical SST changes led to fluctuations in tropical and subtropical SSTs, possibly linked with changing solar radiation distribution in driving ocean and climate variability, and mediated by planetary waves and atmospheric teleconnections, which modulate ocean heat convergence and influence global circulation strength (Clark et al., 2024). These findings likely indicate how alterations in the distribution of solar radiation across different latitudes impact the intensity of heating and cooling within both the Earth's atmosphere and oceans.

Additionally, the sign of obliquity-related insolation forcing changes around ~40° of latitude, accentuating equator-to-poles gradients. The long time delays in causality and the prominent influence of variations in high latitudes over these timescales are likely consequences of how the spatial distribution in surface energy balance influences the strength and scope of ocean circulation patterns, and in particular the thermohaline circulation. These long time delays are coherent with feedbacks between sea ice, albedo, and deep ocean circulation, where high-latitude cooling amplifies ice cover variations, affecting deep-water formation and, consequently, global deep ocean.

Finally, our results indicate that some modes of SST variability may be linked to nonlinear thresholds in ocean circulation, consistent with previous studies suggesting that abrupt AMOC slowdowns can occur in response to freshwater input from glacial melting. Overall, these findings provide new insights into the long-term dynamics of ocean circulation and its connection to the global deep ocean and low-to-high latitudes heat balance.

Our approach provides first insight into causal relationships and the timescales and likely processes involved in past SST and climate variations. Further research may refine understanding of the underlying processes, for example, through application of the same method to long-term model simulations and comparison of the results with our analysis of real-world observations. Finally, this study also highlights the benefits of combining a decomposition method (like MEMD) with a complex-system-based one (like LRT) to gain further insights into the timescale-dependent features of a real-world systems (Alberti, Consolini, et al., 2020; Alberti, Daviaud, et al., 2023; Alberti, De Michelis, et al., 2023; Alberti et al., 2025; Alberti, Faranda, et al., 2023; Alberti, Giannattasio, et al., 2020).

Conflict of Interest

The authors declare no conflicts of interest relevant to this study.

Data Availability Statement

The Sea Surface Temperatures (SST) data used in the study are available as supplementary materials of Clark et al. (2024) as well as in Alberti and Stumpo (2025). The Matlab numerical code used for the multivariate empirical mode decomposition (MEMD) of the SST data is preserved at <https://www.commsp.ee.ic.ac.uk/~mandic/research/emd.htm>, available via Creative Commons Attribution 4.0 International license. The Python numerical code used for the Linear Response (LR) analysis of the multivariate intrinsic mode functions extracted from MEMD of the SST data is preserved at Alberti and Stumpo (2025). The software for reproducing figures is preserved at Alberti and Stumpo (2025).

Acknowledgments

We warmly thank three anonymous reviewers for fruitful suggestions helping us in significantly improving the results presented in this manuscript. Open access publishing facilitated by Istituto Nazionale di Geofisica e Vulcanologia, as part of the Wiley - CRUI-CARE agreement.

References

- Alberti, T., Consolini, G., Ditlevsen, P. D., Donner, R. V., & Quattrociochi, V. (2020). Multiscale measures of phase-space trajectories. *Chaos*, 30(12), 123116. <https://doi.org/10.1063/5.0008916>
- Alberti, T., Daviaud, F., Donner, R. V., Dubrulle, B., Faranda, D., & Lucarini, V. (2023). Chameleon attractors in turbulent flows. *Chaos, Solitons & Fractals*, 168, 113195. <https://doi.org/10.1016/j.chaos.2023.113195>
- Alberti, T., De Michelis, P., Santarelli, L., Faranda, D., Consolini, G., & Marcucci, M. F. (2023). Tracking geomagnetic storms with dynamical system approach: Ground-based observations. *Remote Sensing*, 15(12), 3031. <https://doi.org/10.3390/rs15123031>
- Alberti, T., Donner, R. V., & Vannitsem, S. (2021). Multiscale fractal dimension analysis of a reduced order model of coupled ocean-atmosphere dynamics. *Earth System Dynamics*, 12(3), 837–855. <https://doi.org/10.5194/esd-12-837-2021>
- Alberti, T., Faranda, D., Lucarini, V., Donner, R. V., Dubrulle, B., & Daviaud, F. (2023). Scale dependence of fractal dimension in deterministic and stochastic Lorenz-63 systems. *Chaos*, 33(2), 023144. <https://doi.org/10.1063/5.0106053>
- Alberti, T., Florindo, F., Rohling, E. J., Lucarini, V., & Faranda, D. (2025). Contrasting dynamics of past climate states and critical transitions via dimensional analysis. *Scientific Reports*, 15(1), 13224. <https://doi.org/10.1038/s41598-025-96432-6>
- Alberti, T., Giannattasio, F., De Michelis, P., & Consolini, G. (2020). Linear versus nonlinear methods for detecting magnetospheric and ionospheric current systems patterns. *Earth and Space Science*, 7(7). <https://doi.org/10.1029/2019EA000559>
- Alberti, T., Lepreti, F., Vecchio, A., Bevacqua, E., Capparelli, V., & Carbone, V. (2014). Natural periodicities and Northern Hemisphere-Southern Hemisphere connection of fast temperature changes during the last glacial period: EPICA and NGRIP revisited. *Climate of the Past*, 10(5), 1751–1762. <https://doi.org/10.5194/cp-10-1751-2014>
- Alberti, T., & Stumpo, M. (2025). Supplementary data for cause-and-effect relationships between sea surface temperature changes in different regions during the past 4.5 million years. *Zenodo*. <https://doi.org/10.5281/zenodo.15598471>
- Ashkenazy, Y., & Tziperman, E. (2004). Are the 41 kyr glacial oscillations a linear response to Milankovitch forcing? *Quaternary Science Reviews*, 23(18–19), 1879–1890. <https://doi.org/10.1016/j.quascirev.2004.04.008>
- Ashwin, P., & Ditlevsen, P. (2015). The middle Pleistocene transition as a generic bifurcation on a slow manifold. *Climate Dynamics*, 45(9–10), 2683–2695. <https://doi.org/10.1007/s00382-015-2501-9>
- Baldovin, M., Cecconi, F., & Vulpiani, A. (2020). Understanding causation via correlations and linear response theory. *Physical Review Research*, 2(4), 043436. <https://doi.org/10.1103/PhysRevResearch.2.043436>
- Berends, C. J., Kahler, P., Lourens, L. J., & van de Wal, R. S. W. (2021). On the cause of the mid-Pleistocene transition. *Reviews of Geophysics*, 59(2), e2020RG000727. <https://doi.org/10.1029/2020RG000727>
- Brierley, C. M., Fedorov, A. V., Liu, Z., Herbert, T. D., Lawrence, K. T., & LaRiviere, J. P. (2009). Greatly expanded tropical Warm Pool and weakened Hadley circulation in the early Pliocene. *Science*, 323(5922), 1714–1718. <https://doi.org/10.1126/science.1167625>
- Clark, P. U., Archer, D., Pollard, D., Blum, J. D., Rial, J. A., Brovkin, V., et al. (2006). The middle Pleistocene transition: Characteristics, mechanisms, and implications for long-term changes in atmospheric pCO₂. *Quaternary Science Reviews*, 25(23–24), 3150–3184. <https://doi.org/10.1016/j.quascirev.2006.07.008>
- Clark, P. U., Shakun, J. D., Rosenthal, Y., Köhler, P., & Bartlein, P. J. (2024). Global and regional temperature change over the past 4.5 million years. *Science*, 383(6685), 884–890. <https://doi.org/10.1126/science.adi1908>
- Cramer, B., Miller, K., Barrett, P., & Wright, J. (2011). Late Cretaceous–Neogene trends in deep ocean temperature and continental ice volume: Reconciling records of benthic foraminiferal geochemistry ($\delta^{18}\text{O}$ and Mg/Ca) with sea level history. *Journal of Geophysical Research*, 116(C12), C12023. <https://doi.org/10.1029/2011jgc007255>
- Daruka, I., & Ditlevsen, P. D. (2016). A conceptual model for glacial cycles and the middle Pleistocene transition. *Climate Dynamics*, 46(1–2), 29–40. <https://doi.org/10.1007/s00382-015-2564-7>
- Ditlevsen, P. D., & Ashwin, P. (2018). Complex climate response to astronomical forcing: The middle-Pleistocene transition in glacial cycles and changes in frequency locking. *Frontiers in Physics*, 6, 62. <https://doi.org/10.3389/fphy.2018.00062>
- Emiliani, C. (1955). Pleistocene temperatures. *The Journal of Geology*, 63(6), 538–578. <https://doi.org/10.1086/626295>
- Foster, G. L., Lear, C. H., & Rae, J. W. (2012). The evolution of pCO₂, ice volume and climate during the middle Miocene. *Earth and Planetary Science Letters*, 341, 243–254. <https://doi.org/10.1016/j.epsl.2012.06.007>
- Hays, J. D., Imbrie, J., & Shackleton, N. J. (1976). Variations in the earth's Orbit: Pacemaker of the ice ages. *Science*, 194(4270), 1121–1132. <https://doi.org/10.1126/science.194.4270.1121>
- Herbert, T. D. (2023). The mid-Pleistocene climate transition. *Annual Review of Earth and Planetary Sciences*, 51(1), 389–418. <https://doi.org/10.1146/annurev-earth-032320-104209>
- Herbert, T. D., Dalton, C. A., Liu, Z., Salazar, A., Si, W., & Wilson, D. S. (2022). Tectonic degassing drove global temperature trends since 20 Ma. *Science*, 377(6601), 116–119. <https://doi.org/10.1126/science.abl4353>
- Herold, N., Huber, M., Muller, R. D., & Seton, M. (2012). Modeling the Miocene climatic optimum: Ocean circulation. *Paleoceanography*, 27(1). <https://doi.org/10.1029/2010PA002041>

- Holbourn, A., Kuhnt, W., Clemens, S., Prell, W., & Andersen, N. (2013). Middle to late Miocene stepwise climate cooling: Evidence from a high-resolution deep water isotope curve spanning 8 million years. *Paleoceanography*, 28(4), 688–699. <https://doi.org/10.1002/2013PA002538>
- Huang, N. E., Shen, Z., Long, S. R., Wu, M. C., Shih, H. H., Zheng, Q., et al. (1998). The empirical mode decomposition and the Hilbert spectrum for nonlinear and non-stationary time series analysis. *Proceedings of the Royal Society of London Series A*, 454(1971), 903–998. <https://doi.org/10.1098/rspa.1998.0193>
- Huang, N. E., & Wu, Z. (2008). A review on Hilbert-Huang transform: Method and its applications to geophysical studies. *Reviews of Geophysics*, 46(2), RG2006. <https://doi.org/10.1029/2007RG000228>
- Huybers, P., & Wunsch, C. (2004). A depth-derived Pleistocene age model: Uncertainty estimates, sedimentation variability, and nonlinear climate change. *Paleoceanography*, 19(1), PA1028. <https://doi.org/10.1029/2002PA000857>
- Imbrie, J., Berger, A., Boyle, E. A., Clemens, S. C., Duffy, A., Howard, W. R., et al. (1993). On the structure and origin of major glaciation cycles 2. The 100,000-year cycle. *Paleoceanography*, 8(6), 699–735. <https://doi.org/10.1029/93PA02751>
- Jackson, L. C., Kahana, R., Graham, T., Ringer, M. A., Woollings, T., Mecking, J. V., & Wood, R. A. (2015). Global and European climate impacts of a slowdown of the AMOC in a high resolution GCM. *Climate Dynamics*, 45(11–12), 3299–3316. <https://doi.org/10.1007/s00382-015-2540-2>
- Lenton, T. M., Held, H., Kriegler, E., Hall, J. W., Lucht, W., Rahmstorf, S., & Schellnhuber, H. J. (2008). Tipping elements in the earth's climate system. *Proceedings of the National Academy of Sciences*, 105(6), 1786–1793. <https://doi.org/10.1073/pnas.0705414105>
- Lisiecki, L. E., & Raymo, M. E. (2005). A Pliocene-Pleistocene stack of 57 globally distributed benthic $\delta^{18}\text{O}$ records. *Paleoceanography*, 20(1). <https://doi.org/10.1029/2004pa001071>
- Lovati, G., De Michelis, P., Alberti, T., & Consolini, G. (2023). Unveiling the core patterns of high-latitude electron density distribution at Swarm Altitude. *Remote Sensing*, 15(18), 4550. <https://doi.org/10.3390/rs15184550>
- Meckler, A. N., Sexton, P., Piasecki, A., Leutert, T., Marquardt, J., Ziegler, M., et al. (2022). Cenozoic evolution of deep ocean temperature from clumped isotope thermometry. *Science*, 377(6601), 86–90. <https://doi.org/10.1126/science.abk0604>
- Miller, K. G., Wright, J. D., & Fairbanks, R. G. (1991). Unlocking the ice house: Oligocene-Miocene oxygen isotopes, Eustasy, and margin erosion. *Journal of Geophysical Research*, 96(B4), 6829–6848. <https://doi.org/10.1029/90JB02015>
- Paillard, D., & Parrenin, F. (2004). The Antarctic ice sheet and the triggering of deglaciations. *Earth and Planetary Science Letters*, 227(3–4), 263–271. <https://doi.org/10.1016/j.epsl.2004.08.023>
- Ravelo, A., Andreasen, D. H., Lyle, M., Olivarez Lyle, A., & Wara, M. W. (2004). Regional climate shifts caused by gradual global cooling in the Pliocene epoch. *Nature*, 429(6989), 263–267. <https://doi.org/10.1038/nature02567>
- Ravelo, A., & Hillaire-Marcel, C. (2007). Chapter eighteen the use of oxygen and carbon isotopes of foraminifera in paleoceanography. *Developments in Marine Geology*, 1, 735–764. [https://doi.org/10.1016/S1572-5480\(07\)01023-8](https://doi.org/10.1016/S1572-5480(07)01023-8)
- Rehman, N., & Mandic, D. P. (2010). Multivariate empirical mode decomposition. *Proceedings of the Royal Society of London Series A*, 466(2117), 1291–1302. <https://doi.org/10.1098/rspa.2009.0502>
- Rohling, E., & Cooke, S. (1999). In B. S. Gupta (Ed.), *Stable oxygen and carbon isotope ratios in foraminiferal carbonate shells*. Kluwer Academic Publishers.
- Rohling, E. J., Foster, G. L., Gernon, T. M., Grant, K. M., Heslop, D., Hibbert, F. D., et al. (2022). Comparison and synthesis of Sea-level and deep-sea temperature variations over the past 40 million years. *Reviews of Geophysics*, 60(4), e2022RG000775. <https://doi.org/10.1029/2022RG000775>
- Rohling, E. J., Foster, G. L., Grant, K. M., Marino, G., Roberts, A. P., Tamisiea, M. E., & Williams, F. (2014). Sea-level and deep-sea-temperature variability over the past 5.3 million years. *Nature*, 508(7497), 477–482. <https://doi.org/10.1038/nature13230>
- Rohling, E. J., Medina-Elizalde, M., Shepherd, J. G., Siddall, M., & Stanford, J. D. (2012). Sea surface and high-latitude temperature sensitivity to radiative forcing of climate over several glacial cycles. *Journal of Climate*, 25(5), 1635–1656. <https://doi.org/10.1175/2011JCLI4078.1>
- Rohling, E. J., Yu, J., Heslop, D., Foster, G. L., Opdyke, B., & Roberts, A. P. (2021). Sea level and deep-sea temperature reconstructions suggest quasi-stable states and critical transitions over the past 40 million years. *Science Advances*, 7(26), eabf5326. <https://doi.org/10.1126/sciadv.abf5326>
- Schreiber, T. (2000). Measuring information transfer. *Physical Review Letters*, 85(2), 461–464. <https://doi.org/10.1103/PhysRevLett.85.461>
- Shackleton, N. (1987). Oxygen isotopes, ice volume and sea level. *Quaternary Science Reviews*, 6(3–4), 183–190. [https://doi.org/10.1016/0277-3791\(87\)90003-5](https://doi.org/10.1016/0277-3791(87)90003-5)
- Stumpo, M., Benella, S., Consolini, G., & Alberti, T. (2023). Dynamical information flow within the magnetosphere-ionosphere system during magnetic storms. *Rendiconti Lincei. Scienze Fisiche e Naturali*, 34(1), 1–9. <https://doi.org/10.1007/s12210-022-01114-4>
- Stumpo, M., Consolini, G., Alberti, T., & Quattrocioni, V. (2020). Measuring information coupling between the solar Wind and the magnetosphere-ionosphere system. *Entropy*, 22(3), 276. <https://doi.org/10.3390/e22030276>
- Van Kampen, N. G. (1992). *Stochastic processes in physics and chemistry* (Vol. 1). Elsevier.
- Westerhold, T., Marwan, N., Drury, A. J., Liebrand, D., Agnini, C., Anagnostou, E., et al. (2020). An astronomically dated record of Earth's climate and its predictability over the last 66 million years. *Science*, 369(6509), 1383–1387. <https://doi.org/10.1126/science.aba6853>
- Zachos, J., Pagani, M., Sloan, L., Thomas, E., & Billups, K. (2001). Trends, rhythms, and aberrations in global climate 65 Ma to present. *Science*, 292(5517), 686–693. <https://doi.org/10.1126/science.1059412>